PNAS RESEARCH ARTICLE | DEVELOPMENTAL BIOLOGY

The dynamic duo of microtubule polymerase Mini spindles/XMAP215 and cytoplasmic dynein is essential for maintaining *Drosophila* oocyte fate

Wen Lu[a], Margot Lakonishok[a], and Vladimir I. Gelfand[a,1]

Edited by Allan Spradling, Carnegie Institution for Science, Baltimore, MD; received February 27, 2023; accepted July 11, 2023

In many species, only one oocyte is specified among a group of interconnected germline sister cells. In *Drosophila melanogaster*, 16 interconnected cells form a germline cyst, where one cell differentiates into an oocyte, while the rest become nurse cells that supply the oocyte with mRNAs, proteins, and organelles through intercellular cytoplasmic bridges named ring canals via microtubule-based transport. In this study, we find that a microtubule polymerase Mini spindles (Msps), the *Drosophila* homolog of XMAP215, is essential for maintenance of the oocyte specification. mRNA encoding Msps is transported and concentrated in the oocyte by dynein-dependent transport along microtubules. Translated Msps stimulates microtubule polymerization in the oocyte, causing more microtubule plus ends to grow from the oocyte through the ring canals into nurse cells, further enhancing nurse cell-to-oocyte transport by dynein. Knockdown of *msps* blocks the oocyte growth and causes gradual loss of oocyte determinants. Thus, the Msps-dynein duo creates a positive feedback loop, ensuring oocyte fate maintenance by promoting high microtubule polymerization activity in the oocyte, and enhancing dynein-dependent nurse cell-to-oocyte transport.

microtubule | *Drosophila* | oocyte | dynein | cell fate

Significance

The process of oocyte determination in *Drosophila melanogaster* provides a valuable model system for studying the fundamental mechanisms of cell fate specification and maintenance. In this study, we identified the crucial role of the duo of microtubule polymerase XMAP215/Mini spindles (Msps) and cytoplasmic dynein in this process. Our results reveal that Msps is essential for oocyte growth and cell fate maintenance. Msps transport and concentration in the oocyte are achieved through dynein-dependent transport of *msps* mRNA along microtubules. Translated Msps stimulates microtubule polymerization in the oocyte, which further enhances nurse cell-to-oocyte transport by dynein. This creates a positive feedback loop that ensures the maintenance of a clear oocyte fate selection.

Mature oocytes, also known as eggs, are usually the largest cell of the organism. To achieve such a large cell size, in addition to de novo synthesis of new materials, oocytes acquire mRNAs, proteins, and organelles from the interconnected sister cells (1, 2). In many species, including the classic model organism *Drosophila melanogaster* as well as mammals, oocytes are specified among a group of interconnected cells, called germline cysts, after incomplete cytokinesis (3, 4). The rest of the sister cells transfer cytoplasmic materials to fast-growing oocytes before undergoing apoptosis (5, 6). Therefore, the oocyte selection represents a "winners take all" paradigm. One big standing question is how the oocyte maintains its "winning" position during development.

The ovary of *Drosophila melanogaster* provides a powerful system to address the question of oocyte fate maintenance due to the ample availability of genetic and cell biology tools. Within *Drosophila* ovaries, a germline stem cell divides to produce a cystoblast, which undergoes four rounds of cell divisions with incomplete cytokinesis to generate 16 interconnected sister cells (called cystocytes) connected through intercellular cytoplasmic bridges, the ring canals (Fig. 1*A*) (7). Among the 16 interconnected cystocytes, one cell is specified as an oocyte, and the remaining 15 sister cells undergo endoreplication, becoming polyploid nurse cells to "nurse" the oocyte (8). The oocyte is not randomly determined in the 16-cell cyst; instead, the oocyte is selected between the first two daughter cells (called pro-oocytes) after the first division of the cystoblast. The pro-oocytes, positioned at the center of the germline cyst, are characterized by four ring canals interconnecting with neighboring cells (the dashed orange box, Fig. 1*A*) (9). The selected oocyte and the 15 sister cells are then encapsulated by a layer of somatic epithelial cells, also known as follicle cells, to form an oval structure called the egg chamber (Fig. 1*A*).

Microtubules and microtubule-associated proteins play the key role in oocyte differentiation. The formation of a single microtubule organizing center (MTOC) within the 16-cell cyst is a hallmark of oocyte specification (11, 12). Depolymerization of microtubules by drugs such as colchicine results in the formation of 16 nurse cells and no oocyte in the cyst (11, 13). The centrosomes from nurse cells and the microtubule minus-end-binding protein Patronin are both accumulated in early oocytes (14, 15). The microtubules, in turn, are nucleated from the MTOC in the oocyte and extend their plus-ends into the interconnected nurse cells via the ring canals (Fig. 1*A*) (16, 17). This polarized microtubule network is proposed to be essential for accumulating oocyte-specific factors by transport powered by the major microtubule minus-end-directed motor, cytoplasmic dynein (16).

Author affiliations: [a]Department of Cell and Developmental Biology, Feinberg School of Medicine, Northwestern University, Chicago, IL 60611

Preprint server: A previous version of this manuscript has been uploaded to the open-access preprint server bioRxiv (89).

Author contributions: W.L. and V.I.G. designed research; W.L., M.L., and V.I.G. performed research; W.L. and M.L. analyzed data; and W.L. and V.I.G. wrote the paper.

The authors declare no competing interest.

This article is a PNAS Direct Submission.

[1]To whom correspondence may be addressed. Email: vgelfand@northwestern.edu.

This article contains supporting information online at https://www.pnas.org/lookup/suppl/doi:10.1073/pnas.2303376120/-/DCSupplemental.

Published September 18, 2023.

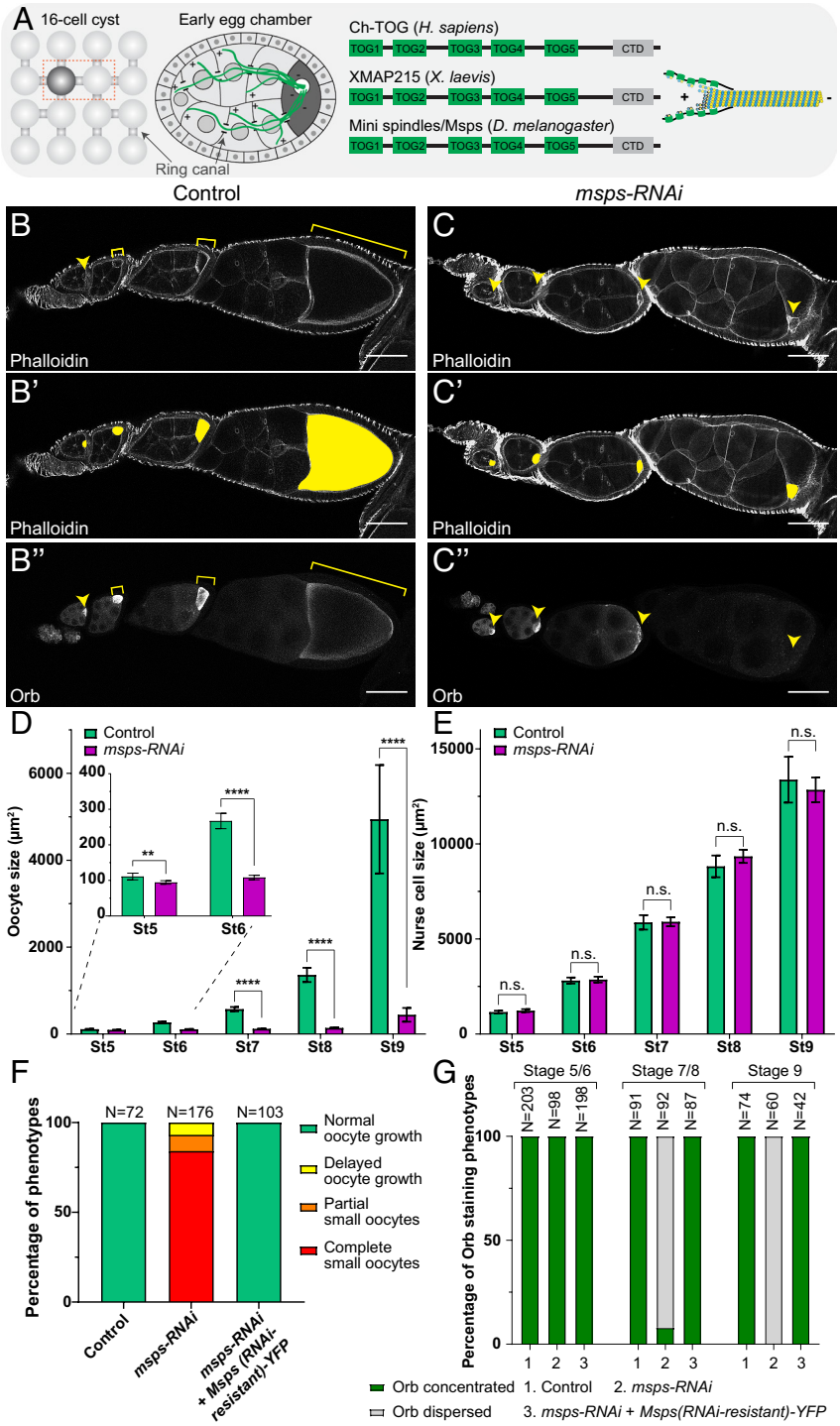

Fig. 1. Msps is required for oocyte growth and cell fate maintenance. (*A*) A cartoon illustration of the oocyte specification in the germline cyst of 16-interconnected cystocytes. The oocyte candidates, the pro-oocytes, are outlined with the dashed orange box. Oo, oocyte. The microtubules in the early egg chamber form a highly polarized network, with minus-ends accumulated in the oocyte and plus-ends extending into the interconnected nurse cells via the ring canals. The XMAP215/Dis1 family is a group of highly conserved microtubule-associated proteins that promote microtubule polymerization in eukaryotes. The homologies in *Drosophila* (Mini spindles, Msps), *Xenopus* (XMAP215), and human (Ch-TOG) all have five TOG domains that interact with either free tubulin dimer or microtubule lattice, and a C-terminal domain (CTD). XMAP215/Msps interacts with the end-binding protein EB1 to track the growing plus-ends of microtubules. (*B–C″*) Phalloidin and Orb staining in control (*B–B″*) and *msps-RNAi* (*C–C″*) ovarioles. Oocytes are highlighted with the yellow arrowheads or brackets (*B–C* and *B″–C″*) or with yellow painting (*B′–C′*). (Scale bars, 50 μm.) (*D* and *E*) Measurements of oocyte size and nurse cell size in stage 5 to stage 9 egg chambers. The oocyte in *msps-RNAi* exhibits a significant decrease in size compared to the control oocytes, starting from stage 5 (*D*). In contrast, the size of nurse cells in *msps-RNAi* is not significantly different from the control (*E*). Sample sizes of control egg chambers: stage 5, N = 75; stage 6, N = 87; stage 7, N = 35; stage 8, N = 28; stage 9, N = 29; *msps-RNAi* egg chambers: stage 5, N = 68; stage 6, N = 93; stage 7, N = 64; stage 8, N = 47; stage 9, N = 59. Data are represented as mean ± 95% CI. Unpaired *t* tests with Welch's correction were performed between control and *msps-RNAi* samples. (*F*) Percentages of oocyte growth phenotypes in the listed genetic background. Classifications of oocyte growth phenotypes were previously described (10). (*G*) Percentages of the Orb staining phenotypes in stage 5 to 6, stage 7 to 8, and stage 9 egg chambers in listed genotypes. Characterizations of Orb concentration and Orb dispersion were previously described (10). (*B–G*) All samples are with one copy of *maternal αtub-Gal4*$^{[V37]}$.

The components of the cytoplasmic dynein complex (hereafter referred to as "dynein"), including dynein heavy chain (Dhc64C), dynein light chain (Dlc), dynein light intermediate chain (Dlic), its key cofactors dynactin and Lissencephaly-1 (Lis1), its activator Bicaudal D (BicD), and its mRNA-binding adaptor Egalitarian (Egl), are all concentrated in the oocyte and are essential for the oocyte specification. Early genetic disruption of these components leads to the lack of oocyte specification in the 16-cell cyst (18–27). Dynein is not only required for oocyte specification but is also indispensable for the maintenance of its differentiation. Later or weaker inhibition of dynein or its cofactors (such as Dhc64C, Dlic, p150/Glued, Lis1, Dlc, and Egl) results in gradual loss of the oocyte identity (10, 22), indicating that maintenance of the oocyte differentiation requires continuous dynein-driven activity.

Intriguingly, dynein is not just working as a minus-end-directed motor along the preformed polarized microtubule network originating from the MTOC in the oocyte; rather, it is involved in organizing and maintaining this polarized network itself. The formation of MTOC is either blocked or disrupted in *BicD* and *egl* mutants (11, 14, 28). BicD is an adaptor that activates the motility of the dynein–dynactin complex and links the complex to its cargoes (29, 30), whereas Egl, an RNA binding protein, serves as a key adaptor for dynein-dependent mRNA transport and is essential for the localization of the polarity determinants (e.g., *oskar*, *gurken*, and *bicoid* mRNAs) in oocytes and early embryos (31–36). However, the mechanism by which dynein regulates microtubule organization in the ovary through BicD and Egl remained elusive.

Microtubules are polymers composed of αβ tubulin dimers. Microtubules can dynamically undergo growing or shrinking. The growth of microtubules can be enhanced by a group of proteins, XMAP215/Dis1 family, that are highly conserved in eukaryotes. The XMAP215 (*Xenopus* microtubule-associated protein 215) was first identified in frog oocytes as a processive microtubule polymerase that stimulates microtubule growth in vitro (37, 38). The higher eukaryotic XMAP215/Dis1 family members, including the *Xenopus* XMAP215, its *Drosophila* homolog Mini spindles (Msps), and the human homolog Ch-TOG, all possess an N-terminal array of five TOG (tumor overexpressed gene) domains (Fig. 1*A*). The TOG domain is composed of six HEAT repeats and forms a flat, paddle-like structure, and the intra-HEAT repeat loops are important for tubulin binding (39–41). The five TOG domains have evolved to have differential preferences for binding either free or polymerized tubulin: TOG1-3 binds to free tubulin dimers, while TOG4-5 prefers tubulin incorporated into the microtubule lattice (42, 43). XMAP215/Msps tracks the plus-ends of growing microtubules (42) via the interaction with the EB1-binding proteins SLAIN2 (44) and Sentin (45). Altogether, XMAP215/Msps uses a polarized array of TOG domains at the microtubule plus-ends and facilitates the addition of soluble tubulin dimers to the microtubule polymer, in which TOG1-2 interact with free tubulin and TOG5 binds to the microtubule lattice-incorporated tubulin, while TOG3-4 bridge and stabilize the intermediate conformation between free and incorporated tubulins (Fig. 1*A*) (42). Knockdown of XMAP215/Msps in *Drosophila* results in shorter or disorganized spindles in mitotic and meiotic cells (46–48). In hypomorphic mutants of *XMAP215/Msps*, the defects in microtubule organization and mRNA localization during mid-oogenesis have been reported (49). However, due to its requirement for spindle formation and mitotic progression, the role of Msps in early oocyte development remained unclear.

Here, we report that *Drosophila* XMAP215/Msps is essential for oocyte growth and cell fate maintenance. Dynein transports and concentrates the *msps* mRNA into the oocyte. As a result, translated Msps protein accumulates in the oocyte and is retained there by its interaction with the oocyte microtubules. Msps promotes microtubule polymerization in the oocyte as well as microtubule growth from the minus-ends in the oocyte into nurse cells. The oocyte concentration of Msps increases the number of plus-end-out microtubules in the ring canals from the oocyte to interconnected nurse cells, further increasing dynein-dependent transport toward the oocyte. Therefore, Msps and dynein form a positive feedback loop that ensures more microtubules originate in the oocytes, and dynein transports more oocyte-specific mRNAs, proteins, and organelles into the oocyte. The dynamic duo together maintains oocyte fate determination by promoting high microtubule polymerization activity in the oocyte and enhancing nurse cell-to-oocyte transport.

Results

XMAP215/Msps Is Essential for Oocyte Growth and Cell Fate Maintenance. The high microtubule polymerization in the oocyte has been well documented both in early (15) and mid-oogenesis (50). Here, we aim to understand how this high microtubule polymerization activity is achieved. We tested the role of a microtubule polymerase, XMAP215/Msps, in the *Drosophila* germ line. As XMAP215/Msps is required for proper mitotic spindle formation, knockdown of Msps by an RNAi line under an early germline driver, *nanos-Gal4*$^{[VP16]}$ that is expressed in the primordial germ cells (51), results in a complete germless ovary (*SI Appendix*, Fig. S1 *A–C*). To bypass the requirement of Msps in cell division, we employed a postmitotic germline-specific driver, *maternal α-tubulin-Gal4*$^{[V37]}$, that drives the expression in egg chambers starting at stages 3 to 4, after the completion of cystocyte cell division (10, 31, 50). The postmitotic knockdown of XMAP215/Msps caused complete oocyte growth arrest in most ovarioles (Fig. 1 *B–F* and *SI Appendix*, Fig. S1*D*). The oocyte remains small and fails to acquire cytoplasmic contents from the interconnected nurse cells (hereafter referred to as the 'small oocyte' phenotype). Interestingly, the oocyte marker, Orb (oo18 RNA-binding protein) (52) is properly concentrated in the oocyte during early oogenesis, but this selective concentration is lost in mid-oogenesis (Fig. 1 *C–C"* and *G*). Furthermore, we used the staining of synaptonemal complex (SC) between homologous chromosomes as a meiosis marker in *Drosophila* oocytes (53, 54) and found that in *msps-RNAi* ovarioles, small oocytes enter meiosis properly in early stages but start to fall out of meiosis starting stage 8 (*SI Appendix*, Fig S1 *E–F'*). Together, these data indicate that *msps-RNAi* driven by *maternal α-tubulin-Gal4*$^{[V37]}$ does not interfere with the early oocyte specification but affects the oocyte fate maintenance.

To ensure that the small oocyte and oocyte cell fate loss are specific to the *msps* knockdown, we generated a YFP-labeled full-length Msps that carries silent mutations making it resistant to the RNAi line we used. This RNAi-resistant Msps-YFP was able to fully rescue the small oocyte and oocyte fate loss phenotypes caused by *msps-RNAi* (Fig. 1 *F* and *G* and *SI Appendix*, Fig. S1 *G* and *G'*), indicating that the oocyte growth and maintenance defects are caused specifically by the lack of Msps, rather than off-target effects of *msps-RNAi*.

XMAP215/Msps Promotes Microtubule Polymerization in the Oocyte. Msps belongs to the XMAP215 protein family and has been shown to promote microtubule polymerization in *Drosophila* cells (42, 43). Having confirmed that Msps is required for oocyte growth and cell fate maintenance, we proceed to examine the effect of *msps-RNAi* on microtubules in the germ line. We used

live imaging of EB1, the end-binding protein 1 that tracks the polymerizing microtubule plus-ends (55), as a readout of microtubule polymerization. An EB1-GFP line under a *ubiquitin* promoter (*ubi-EB1-GFP*) (50, 56–58) showed that in control egg chambers, the microtubule polymerization activity is much higher in the oocyte than in nurse cells (Fig. 2 *A*, *C*, and *D*) (Movie S1). This high microtubule polymerization activity results in more microtubule plus-ends growing from the oocyte into nurse cells (Movie S2), which is important for establishing the polarized microtubule network for nurse-to-oocyte transport (Fig. 1*A*). Knockdown of *msps* by RNAi leads to a drastic reduction of EB1 tracks in the oocytes and nurse cells, as well as in the nurse cell-to-oocyte ring canals (Fig. 2 *B–D*) (Movie S3). As a result, the amount of microtubules in the *msps-RNAi* oocyte is severely reduced compared to the control oocyte, as seen by both tubulin antibody staining of fixed ovaries and the in vivo microtubule labeling with the GFP-tagged microtubule-binding domain of Ensconsin/MAP7 (EMTB-3XGFP) (10) (Fig. 2 *E–G* and *SI Appendix*, Fig. S2 *A–C*). Very intriguingly, the microtubule level in nurse cells is largely unaffected (Fig. 2 *E, F*, and *H* and *SI Appendix*, Fig. S2 *A*, *B*, and *D*), suggesting that most microtubules in nurse cells are either stable and do not rely on microtubule dynamics, or use a factor other than Msps to promote tubulin polymerization. Together, these data show that Msps is the main factor driving high microtubule polymerization activity in the oocyte.

To further investigate the role of high microtubule polymerization activity in the oocyte fate, we used GFP-tagged Klp10A, the *Drosophila* kinesin-13 known to depolymerize microtubules in *Drosophila* cells (59–61). Overexpression of Klp10A in the ovary driven by *maternal αtub-Gal4*$^{[V37]}$ leads to significant microtubule loss both in the oocyte and nurse cells and results in the majority of the ovarioles having small oocytes and gradually losing oocyte fate, phenocopying the *msps-RNAi* mutant (*SI Appendix*, Fig. S2 *E–I*). It suggested that the loss of microtubules is the main reason attributed to the defects in oocyte growth and cell fate maintenance observed in *msps-RNAi*.

***XMAP215/msps* mRNA is Concentrated in the Oocyte by Dynein-Dependent Transport.** How does Msps selectively regulate microtubule polymerization in the oocyte? Previous data suggested that *msps* mRNA is localized in the oocytes (49). We decided to better visualize *msps* mRNA using single-molecule inexpensive fluorescence in situ hybridization (smiFISH) and found that *msps* mRNA is indeed highly concentrated in the oocytes (Fig. 3 *A* and *A'*). The smiFISH signal is specific to *msps* mRNA as germline knockdown of *msps* by RNAi leads to a complete abolishment of the smiFISH signal of *msps* RNA (*SI Appendix*, Fig. S3 *A–B'*).

Next, we demonstrated that the *msps* mRNA accumulation in the oocyte is dependent on dynein. Knockdown of dynein heavy chain (Dhc64C), dynein light intermediate chain (Dlic), or Lis1 all results in the "small oocyte" phenotype as previously described (10) and drastically reduces the amount of *msps* mRNA in the oocytes (Fig. 3 *B*, *B'*, *D*, and *E* and *SI Appendix*, Fig. S3 *C–D'*). The reduction of *msps* mRNA accumulation becomes more prevalent starting at stage 5, which is consistent with the fact that the *maternal αtub-Gal4*$^{[V37]}$ driver used to express RNAi starts its expression around stage 3 to 4 (31). Furthermore, we found that a dynein adaptor Egalitarian (Egl) plays an essential role in localizing *msps* mRNA to the oocyte. Egl is known to be important for linking multiple mRNAs to the dynein motor complex (34) and is essential for oocyte development and mRNA localization (22, 31). Knockdown of Egl by RNAi driven by *maternal αtub-Gal4*$^{[V37]}$ leads to a significantly reduced *msps* mRNA level in the oocyte (Fig. 3 *C–E*), suggesting that Egl is essential for linking the mRNA to the dynein complex. Interestingly,

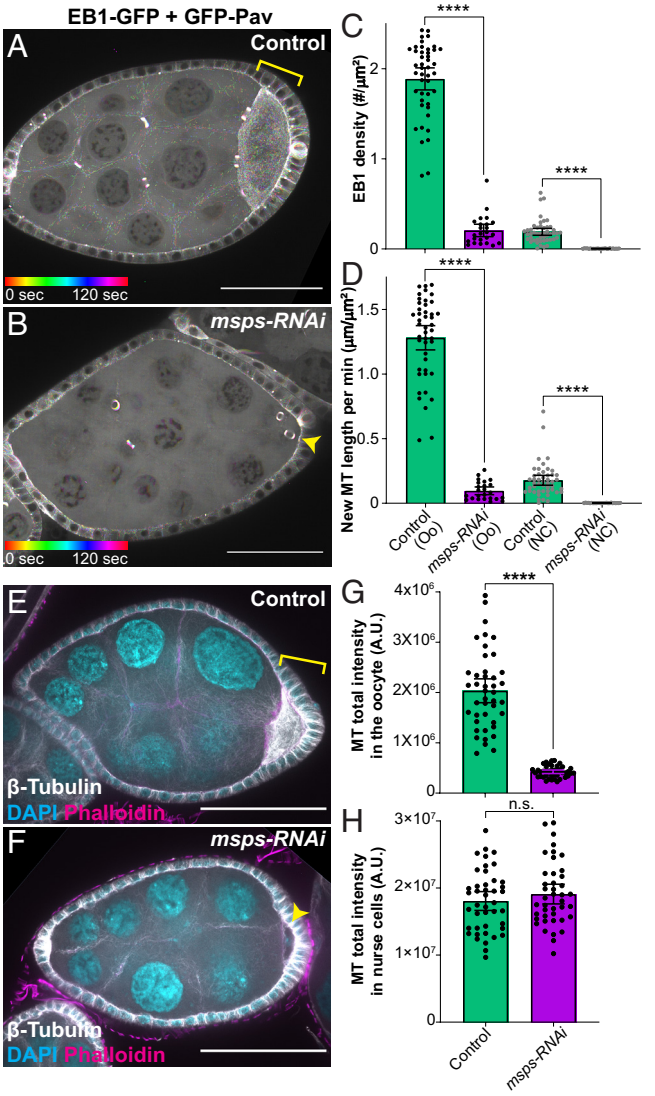

Fig. 2. Msps promotes microtubule polymerization in the oocyte. (*A* and *B*) Temporal color-coded hyperstacks of *ubi*-EB1-GFP in control (*A*) and *msps-RNAi* (*B*). In control, more polymerizing microtubule plus-ends were seen in the oocyte than in nurse cells, indicated by the colored tracks (*A*). In *msps-RNAi*, very few EB1 comets can be seen in the oocyte and nurse cells (*B*). In addition to *ubi*-EB1-GFP, a GFP-tagged Pavarotti/kinesin-6 under an *ubi* promoter (*ubi*-GFP-Pav) was used to illustrate the positions of ring canals. (*C* and *D*) Quantification of the density of EB1 comets and the length of newly polymerized microtubules in stage 6 to 8 egg chambers of control and *msps-RNAi*. Oo, oocyte, black dots; NC, nurse cells, gray dots. (*E–H*) Representative images (*E* and *F*) and quantifications (*G* and *H*) of microtubule staining in control and *msps-RNAi* stage 6 to 7 egg chambers. Total microtubule intensity in *msps-RNAi* oocytes is heavily diminished compared to control oocytes (*G*), while nurse cell microtubules are not largely affected by the *msps* knockdown (*H*). A.U., Arbitrary Unit. (*A–H*) All samples are with one copy of *maternal αtub-Gal4*$^{[V37]}$. (*A*, *B*, *E*, and *F*) Microtubule dynamics and staining pattern are not affected in the somatic follicle cells of *msps-RNAi* samples, as *msps-RNAi* is only driven in germline cells. Oocytes are indicated by the yellow arrowheads or brackets. (Scale bars, 50 μm.) (*C*, *D*, *G*, and *H*) Data are represented as scattered individual data points with mean ± 95% CI. Unpaired *t* tests with Welch's correction were performed between control and *msps-RNAi* samples. See more details in Materials and Methods "EB1 comet tracking in *Drosophila* egg chambers" and "Quantification of microtubule staining in *Drosophila* egg chambers".

despite the heavily reduced *msps* mRNA in the oocyte, the *egl-RNAi* oocyte is significantly larger than the *Dhc-RNAi* ones (*SI Appendix*, Fig. S3*E*). Noticeably, the oocyte-to-nurse cell ratio of *msps* mRNA average intensity is significantly higher in *egl-RNAi* than in *Dhc-RNAi* (*SI Appendix*, Fig. S3*F*), suggesting that the relative abundance of *msps* mRNA could be the key to maintain oocyte determination and promote oocyte growth.

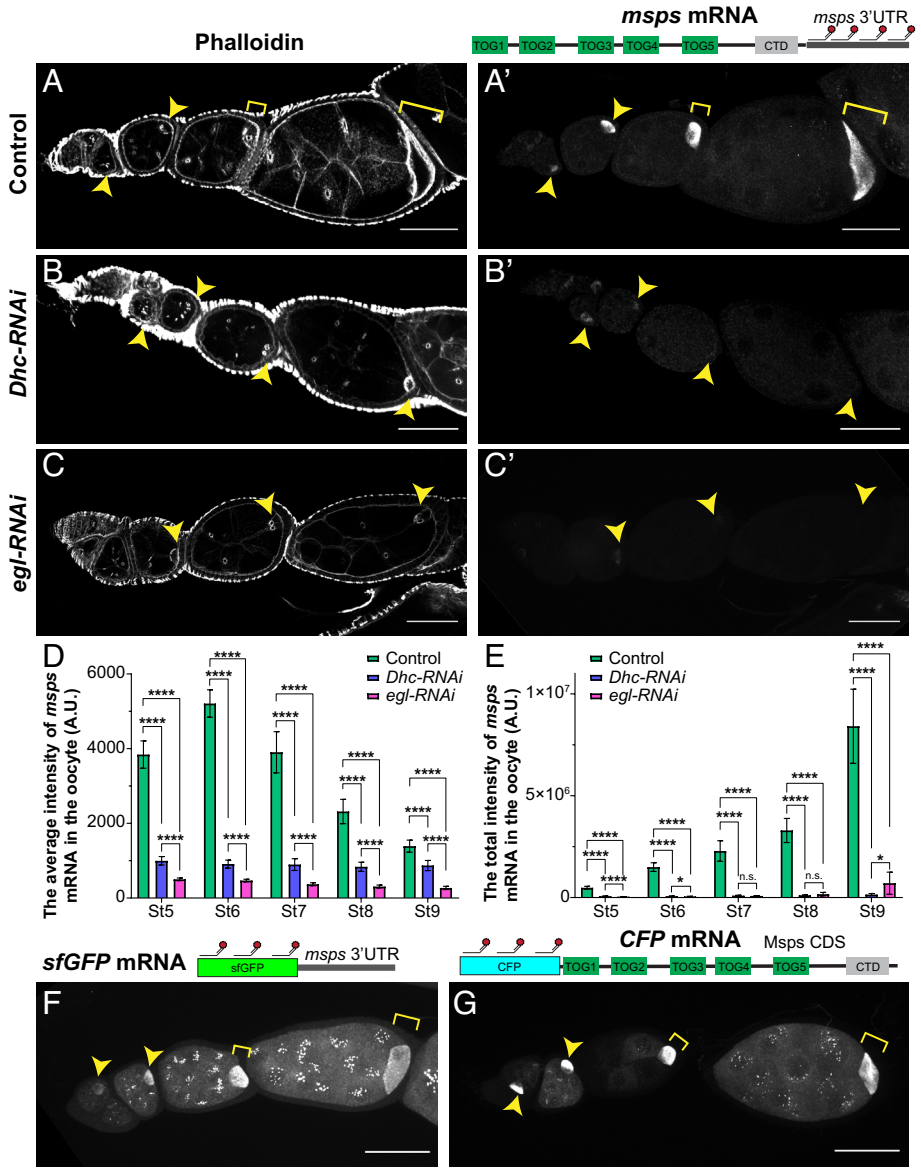

Fig. 3. Dynein is required for *msps* mRNA concentration in the oocyte. (*A–C'*) Phalloidin and smiFISH staining of *msps* mRNA in control (*A* and *A'*), *Dhc-RNAi* (*B* and *B'*), and *egl-RNAi* (*C* and *C'*). Cy5-labeled FLAP-X smiFISH probes recognize the 3'UTR of *msps* mRNA. *msps* mRNA is concentrated in control oocytes, but heavily reduced in *Dhc-RNAi* and *egl-RNAi* oocytes. (*D* and *E*) Average and total fluorescence intensity of *msps* mRNA (by smiFISH against *msps* 3'UTR) in control, *Dhc-RNAi*, and *egl-RNAi*. The sample sizes of control oocytes: stage 5, N = 38; stage 6, N = 41; stage 7, N = 19; stage 8, N = 23; stage 9, N = 24; *Dhc-RNAi* oocytes: stage 5, N = 54; stage 6, N = 47; stage 7, N = 38; stage 8, N = 32; stage 9, N = 30; *egl-RNAi* oocytes: stage 5, N = 71; stage 6, N = 56; stage 7, N = 55; stage 8, N = 32; stage 9, N = 25. (*F* and *G*) The mRNA localizations of *sfGFP-msps 3'UTR* (*F*) and *CFP-Msps.CDS* (*G*) via the Cy5-labeled FLAP-X smiFISH probes against sfGFP and CFP, respectively. Both mRNAs show clear oocyte enrichments. All samples are with one copy of *maternal αtub-Gal4*$^{[V37]}$. (*A–C'*, *F*, and *G*) Oocytes are indicated by the yellow arrowheads or brackets. A small (5 μm) (*A–C'*) or a large (>25 μm) (*F* and *G*) Max-intensity Z projection was used to show the mRNA localization. (Scale bars, 50 μm.) (*D* and *E*) Data are represented as mean ± 95% CI and unpaired *t* tests with Welch's correction were performed.

We tested which subregion of *msps* mRNA is required to drive the mRNA accumulation in the oocyte. It turned out that either the coding sequence (CDS) or the 3' untranslated region (3'-UTR) is sufficient to localize to the mRNA into the oocyte (Fig. 3 *F* and *G*), while a standard 3'-UTR used in the germline transformation vector results in most mRNAs staying in the nurse cells (*SI Appendix*, Fig. S3 *G* and *G'*). Knockdown of dynein eliminates both the CDS and 3'UTR mRNA accumulation in the oocyte (*SI Appendix*, Fig. S3 *H* and *I*). This is quite different from a single RNA stem-loop structure used as the dynein-dependent localization signal in *K10* (transport/localization sequence, TLS), *gurken* (GLS), *I-factor Retrotransposon* (ILS), and *hairy* (SL1) via the interaction with Egl (34, 62–64). It implies that *msps* mRNA may employ a different mechanism for interaction with Egl and the dynein motor.

XMAP215/Msps Protein Is Retained in the Oocyte Via Microtubule Interaction. To examine the localization of Msps protein in the germ line, we generated a CRISPR knock-in line using the NanoTag epitope, VHH05 (65). We inserted three copies of VHH05 at the C-terminal end of the coding region (Fig. 4*A* and *SI Appendix*, Fig. S4 *A* and *B*). This insertion does not affect the protein functionality as the homozygotes of the CRISPR knock-in line (Msps-3XVHH05) are completely viable and fertile. Coexpression with an EGFP-tagged nanobody specifically recognizing VHH05 (NbVHH05-EGFP) (65) shows that Msps protein is accumulated in the oocytes by a dynein-dependent mechanism (Fig. 4 *B–F*), similar to *msps* mRNA (Fig. 3). This Msps protein enrichment in the oocyte is consistent with a previous report using an antibody against Msps (49) and is further confirmed here using a different anti-Msps antibody (43) (*SI Appendix*, Fig. S5*A*), C-terminally

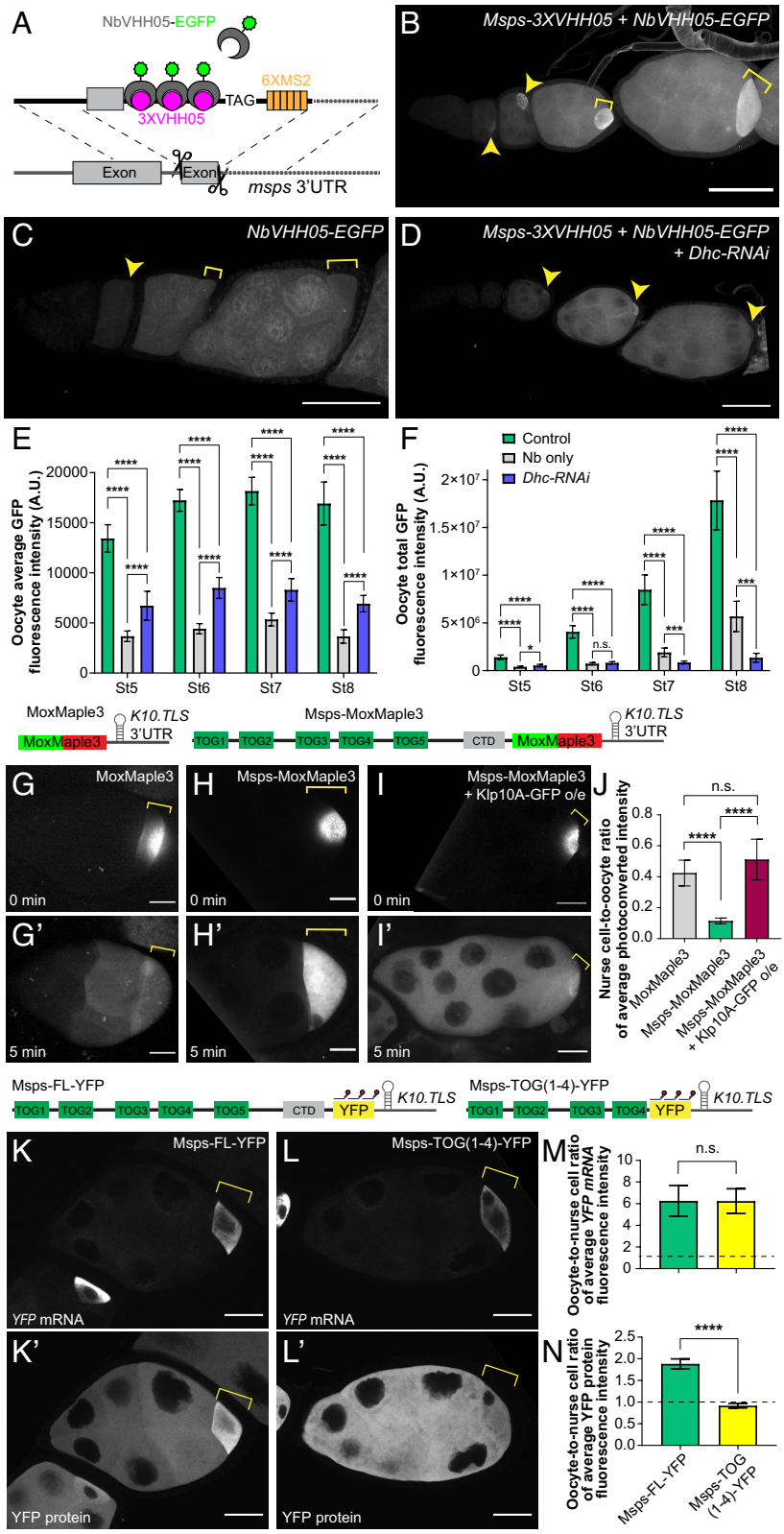

Fig. 4. Msps protein is retained in the oocyte via microtubule interaction. (*A*) A schematic illustration of labeling Msps protein with the nanotag VHH05. Three copies of VHH05 epitope tags are inserted at the C terminus of Msps CDS via CRISPR-mediated homologous recombination. An EGFP-tagged nanobody specifically recognizing the VHH05 epitope (NbVHH05-EGFP) is expressed to visualize the Msps protein localization. (*B–D*) Msps protein localization in control (*Msps-3XVHH05 + NbVHH05-EGFP*) (*B*), nanobody only (*NbVHH05-EGFP*) (*C*), and *Dhc-RNAi* (*Msps-3XVHH05 + NbVHH05-EGFP + Dhc-RNAi*) (*D*). (*E* and *F*) Average and total fluorescence intensity of NbVHH05-EGFP in control, nanobody only, and *Dhc-RNAi*. (*E*) The sample sizes of control oocytes: stage 5, N = 31; stage 6, N = 37; stage 7, N = 27; stage 8, N = 11; Nanobody (Nb) only oocytes: stage 5, N = 17; stage 6, N = 15; stage 7, N = 17; stage 8, N = 9; *Dhc-RNAi* oocytes: stage 5, N = 18; stage 6, N = 25; stage 7, N = 16; stage 8, N = 18. (*G–I'*) Photoconverted signal of MoxMaple3 (*G* and *G'*), Msps-MoxMaple3 (*H* and *H'*), and Msps-MoxMaple3 with Klp10A-GFP overexpression (*I* and *I'*) at 0 min (*G–I*) and 5 min (*G'–I'*) after local photoconversion in the oocyte. K10 SubregionA containing the dynein-dependent localization signal (*K10.TLS*) (62) was inserted at the beginning of the 3'-UTR to ensure the mRNA enrichment in the oocyte. (*J*) The nurse cell-to-oocyte ratio of the average fluorescence intensity of the red photoconverted signal in stage 7 to 8 egg chambers. For MoxMaple3, N = 17; for Msps-MoxMaple3, N = 19; for Msps-MoxMaple3 + Klp10A-GFP overexpression, N = 10. (*K* and *L'*) The distribution of YFP mRNA and protein of ectopically expressed Msps-Full-length (FL)-YFP (*K* and *K'*) and Msps-TOG(1-4)-YFP (*L* and *L'*). Cy5-labeled FLAP-X smiFISH probes recognizing the YFP coding region were used to visualize *YFP* mRNA. (*M* and *N*) The oocyte-to-nurse cell ratio of average fluorescence intensity of YFP mRNA (*M*) and YFP protein (*N*) in stage 7 to 8 egg chambers expressing Msps-FL-YFP (N = 26) and Msps-TOG(1 to 4)-YFP (N = 23). The dashed line represents a uniform distribution of fluorescence intensity between nurse cells and the oocyte. All samples are with one copy of *maternal αtub-Gal4*$^{[V37]}$. Oocytes are indicated by the yellow arrowheads or brackets. (Scale bars, 50 μm (*B–D*) and 25 μm (*G–I'* and *K–L'*).) Data are represented as mean ± 95% CI and unpaired *t* tests with Welch's correction were performed (*E*, *F*, *J*, *M*, and *N*).

tagged Msps-YFP (*SI Appendix*, Fig. S1*G'*) and Msps-GFP (66) (*SI Appendix*, Fig. S5*B*), and an N-terminally tagged CFP-Msps (67) (*SI Appendix*, Fig. S5 *C* and *D*).

However, the mRNA accumulation in the oocyte alone is not sufficient to maintain a high concentration of a soluble protein pool in the oocyte. For example, adding a dynein-dependent localization signal of *K10* (*K10.TLS*) (62) in the 3'UTR region of the mRNA encoding a photoconvertible protein, MoxMaple3, is sufficient to concentrate this mRNA in the oocyte (*SI Appendix*, Fig. S5*E*). However, as the oocyte and nurse cells are interconnected via ring canals, red fluorescent signal of the soluble MoxMaple3 photoconverted in the oocyte rapidly diffuses back into nurse cells (Fig. 4 *G*, *G'*, and *J*). As a result, MoxMaple3 protein can be seen throughout the whole egg chamber after localized translation (*SI Appendix*, Fig. S5*E'*). Similarly, the translated product of the soluble sfGFP with *msps 3'UTR* is not restricted

to the oocyte, even though its mRNA is concentrated in the oocyte (*SI Appendix*, Fig. S5 *F* and *F'*).

Thus, in addition to the localized translation, an active retention mechanism is required to keep a high Msps protein concentration in the oocyte. It is supported by the fact that the photoconverted fusion protein Msps-MoxMaple-*K10.TLS* remains mostly restricted to the oocyte after photoconversion, unlike MoxMaple-*K10.TLS* alone (Fig. 4 *G–H'* and *J*). As Msps interacts with the microtubule lattice and polymerizing plus-ends (42, 43, 45), we speculated that microtubules in the oocyte play a role in the retention of Msps protein, preventing its diffusion into nurse cells. To test this hypothesis, we depolymerized microtubules in the oocyte by Klp10A-GFP overexpression (*SI Appendix*, Fig. S2 *F–I*). We performed the same photoconversion experiments in these Klp10A-overexpressing ovaries; instead of being retained in the oocyte, Msps-MoxMaple3 rapidly diffuses into the interconnected nurse cells from a microtubule-free oocyte (Fig. 4 *I* and *J*). It indicates that the presence of microtubules is crucial for maintaining the concentration of Msps protein in the oocyte.

A previous study demonstrated that a Msps truncation consisting of the first four TOG domains, known as TOG(1–4), lacks the microtubule lattice interaction domain, and as a result, it loses its ability to interact with and decorate microtubules in *Drosophila* S2 cells (43). We compared the mRNA and protein localization of the ectopically expressed YFP-tagged Msps-FL and Msps-TOG(1–4). mRNA transcripts of both Msps constructs were found to be concentrated in the oocytes (Fig. 4 *K–L* and *M*). However, while the Msps-FL protein exhibited a distinct oocyte-concentrated pattern, the Msps-TOG(1–4) protein displayed no preference between nurse cells and the oocyte (Fig. 4 *K'–L'* and *N*). Collectively, our results demonstrate that microtubule binding is essential for retaining Msps protein in the oocyte after localized translation.

Discussion

Altogether, we have shown that 1) dynein transports *msps* mRNA into the oocyte; 2) translated Msps protein is retained in the oocyte in a microtubule-dependent mechanism; 3) Msps protein accumulated in the oocyte assembles the polarized oocyte-to-nurse cell microtubule network, which promotes dynein-dependent transport toward the oocyte. Thus, Msps and dynein form a positive feedback loop to ensure that the oocyte has a higher microtubule polymerization activity and thus more minus-ends-in microtubules than nurse cells (Fig. 5 and Movie S4). Therefore, the Msps-dynein dynamic duo team is essential for oocyte growth and oocyte fate maintenance.

Egl Links *msps* mRNA to the Dynein Complex and Regulates Microtubule Dynamics. Egl is a dynein adaptor essential for linking mRNAs to the dynein motor. Egl has BicD-binding and Dlc-binding domains at the oppositive ends of the molecule and a central mRNA-binding domain (22, 27, 34). Dlc binding facilitates Egl dimerization and thus mRNA binding; in turn, Egl-mRNA binds BicD and gets attached to the dynein complex (32, 35, 68). We found that *msps* mRNA accumulation requires both dynein and the RNA-binding Egl, suggesting that Egl links *msps* mRNA to dynein for dynein-dependent transport into the oocyte. Unlike most of the well-known Egl binding mRNA cargoes (e.g., *K10*, *gurken*, *I-factor Retrotransposon*, and *hairy*), *msps* mRNA has more than a single dynein localization signal, as both *msps* CDS mRNA and 3'UTR mRNA are transported into the oocyte in a dynein-dependent manner (Fig. 3 *F* and *G* and *SI Appendix*, Fig. S3 *H* and *I*). Further studies of narrowing down the dynein-dependent localization signals in the *msps* coding region and the 3'UTR are required to dissect the interaction mechanism. Recently, the positively charged region within the Egl RNA binding domain responsible for binding the localization element of the *I* factor Retrotransposon (ILS) has been mapped (33). Therefore, it would be interesting to test whether this Egl region is also required for interacting with *msps* mRNA.

Previously, it has been shown that the formation of the MTOC in the oocyte is disrupted in *BicD* and *egl* mutants (11, 14, 28), indicating that dynein and Egl are actively involved in organizing and maintaining the polarized oocyte microtubule network. Based on our study, the key player in the process is XMAP215/Msps: *msps* mRNA is transported by dynein to the oocyte via its interaction with Egl and then translated to Msps protein, which in turn stimulates microtubule formation in the oocyte.

Msps Protein Retention in the Oocyte is Microtubule-Dependent. Our data suggest that the *msps* mRNA concentration in the oocyte is not sufficient to maintain its protein accumulation in the oocyte, as soluble MoxMaple3 or sfGFP produced in the oocyte from localized mRNA diffuses to nurse cells through the ring canals (Fig. 4 *G* and *G'* and *SI Appendix*, Fig. S5 *E–F'*). Thus, an active retention mechanism is required to keep produced Msps protein in the oocyte. Since Msps binds microtubule lattice and polymerizing plus-ends (42, 43, 45), we hypothesized that the interaction between Msps and microtubules is a key to its retention in the oocyte. We took advantage of the established Klp10A-GFP overexpression line that depolymerizes most of the microtubules in the oocyte and, as a result, decreases the oocyte size (*SI Appendix*, Fig. S2 *E–I*). The oocyte-photoconverted Msps-MoxMaple3 is seen throughout the

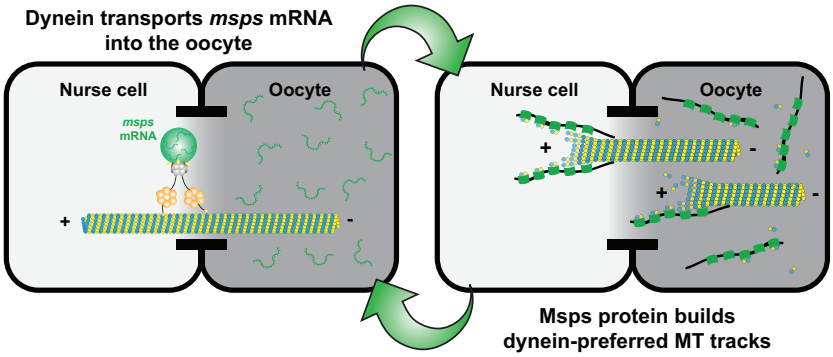

Fig. 5. The Msps-dynein positive feedback loop ensures the oocyte determination. The positive feedback loop is driven by the Msps-dynein duo team: dynein transports *msps* mRNA into the oocyte, while the localized translation of Msps protein promotes microtubule polymerization with plus-ends extending into the nurse cell, which creates dynein-preferred walking tracks. Together, it ensures the highest microtubule polymerization activity in the oocyte and promotes nurse cell-to-oocyte transport, which maintains a clear oocyte fate determination.

entire egg chamber after microtubule depolymerization (Fig. 4 *I–J*). It indicates that in the absence of microtubules, Msps protein is no longer retained within the oocyte after localized translation. Interestingly, with Klp10A overexpression, oocyte-photoconverted Msps-MoxMaple3 protein very often does not display the tiering pattern (the posterior nurse cells have more photoconverted signal than the anterior nurse cells) that we observed in the MoxMaple3 control samples (compare Fig. 4 *I'* to *G'*). We speculate that the different pattern observed with Klp10A overexpression is owing to the decrease in microtubule density, which can lower viscosity of the cytoplasm and reduce diffusion barriers, allowing for further diffusion of proteins among germline cells.

In addition, we employed a Msps truncation known as Msps-TOG(1–4), which lacks the ability to interact with the microtubule lattice (43). Our results clearly showed that compared to the full-length construct, Msps-TOG(1–4) fails to be retained within the oocyte following localized translation (Fig. 4 *K–N*). This finding strongly supports our hypothesis that the interaction between Msps and microtubules is crucial for its retention in the oocyte. Interestingly, previous studies have demonstrated that this Msps-TOG(1–4) truncation largely rescues microtubule polymerization in *Drosophila* S2 cells, while the TOG5 and the linker domain between TOG4 and TOG5 are essential for its association with microtubule lattice (43, 69). These findings propose an intriguing possibility that Msps consists of two distinct modules: the N-terminal module, required for microtubule polymerization function, and the C-terminal module, crucial for proper cellular localization.

The Difference in Microtubule Stability between Nurse Cells and the Oocyte. Microtubules exhibit distinct patterns of polymerization activity between nurse cells and the oocyte (Fig. 2 and Movie S1). Very likely, the dynamics of microtubules in nurse cells and the oocyte are regulated by different mechanisms. The high XMAP215/Msps level promotes a higher level of microtubule polymerization in the oocyte compared to nurse cells. At the same time, microtubules in nurse cells are significantly more stable than the oocyte. Previously, we have shown that the photoconverted microtubules persist in nurse cells for more than 20 min without significant subunit exchange (10), but microtubules photoconverted in the oocytes before stage 10B undergoes very fast depolymerization and repolymerization (70). This explains a very small difference in microtubule amount in nurse cells between control and *msps-RNAi*, as nurse cell microtubules are stable and likely independent of Msps-mediated polymerization. It raises a possibility that, in addition to the oocyte-concentrated microtubule polymerase XMAP215/Msps, a distinct mechanism stabilizes microtubules in nurse cells, and components of this mechanism are excluded from the oocyte. More studies are needed to characterize the different profiles of the microtubules in nurse cells and the oocyte and gain a better understanding of the differential regulations of these microtubule populations.

The Positive Feedback Loop can Amplify the Initial Difference in Microtubule Polarity. Having established that Msps-dynein duo maintains the "winning" position of the oocyte, we propose that it also plays an important role in selecting the "winner" between two pro-oocytes. We speculate that the positive feedback loop transforms a small initial difference in microtubule polarity between two pro-oocytes into a uniform microtube polarity with most minus-ends in the winning oocyte.

The initiation of this positive feedback loop requires that one of the cystocytes have a slightly higher concentration of microtubule minus-ends. Among the 16 cystocytes within the *Drosophila* germline cyst, only the two oldest cells, the pro-oocytes, compete to become the oocyte. It has been shown that the pro-oocytes inherited slightly more materials of the fusome, an interconnecting structure enriched with membrane vesicles, actin, and spectrin, than other sister cells (15). Hence, the pro-oocytes are born with more minus-end stabilizing protein, Patronin/CAMSAP, that is recruited to the fusome structure via interacting with the spectraplakin protein, Short stop (15). Furthermore, the centrosomes are accumulated in the future oocytes after migrating along the fusome, providing further advantages of minus-end nucleating activity over other sister cells (71).

A slight stochastic difference in the density of microtubule minus-ends between two pro-oocytes may occur after cell division (72). The Msps-dynein positive feedback loop can then amplify this small initial difference and transform one of the two pro-oocytes into the "winning" oocyte, promoting microtubule polymerization and enhancing nurse cell-to-oocyte transport.

Materials and methods

***Drosophila* Husbandry and Maintenance.** Fly stocks and crosses were kept on standard cornmeal food (Nutri-Fly Bloomington Formulation, Genesee, Cat # 66-121) supplemented with active dry yeast in the 24 °C incubator. Following flies were used in this study: *mat αtub-Gal4$^{[V37]}$* (III, Bloomington *Drosophila* Stock Center #7063); *nos-Gal4$^{[VP16]}$* (III) (51, 73); *UAS-msps-RNAi* (HMS01906, attP40, II, Bloomington *Drosophila* Stock Center # 38990, targeting Msps CDS 5001-5021 nt, 5′- CTGCGCGACTATGAAGAAATA-3′); *ubi-EB1-GFP* (III) (from Dr. Steve Rogers, the University of North Carolina at Chapel Hill) (50, 56–58); *UASp-EB1-GFP* (II, from Dr. Antoine Guichet, CNRS, Institut Jacques Monod) (50, 74); *ubi-GFP-Pav* (II, from Dr. David Glover, Caltech) (50, 75); *mat αtub67C-EMTB-3XGFP-sqh 3′UTR* (attP40, II, from Dr. Yu-Chiun Wang, RIKEN Center for Biosystems Dynamics Research) (10); *UASp-Klp10A-GFP-SspB* (II) (61); *UAS-Dhc64C-RNAi* (TRiP.GL00543, attP40, II, Bloomington *Drosophila* Stock Center #36583, targeting DHC64C CDS 10044–10,064 nt, 5′-TCGAGAGAAGATGAAGTCCAA-3′) (10, 56, 57); *UAS-Dlic-RNAi* (targeting Dlic 3′UTR 401 to 421 nt, 5′-AGAAATTTAACAAAAAAAAAA-3′, III, inserted at VK05 75A10 site) (10); *UAS-Lis1-RNAi* (II, from Dr. Graydon Gonsalvez, Augusta University, targeting Lis1 CDS 1197–1217 nt, 5′-TAGCGTAGATCAAACAGTAAA-3′) (10, 76); *UAS-Egl-RNAi* (TRiP.GL01170, attP2, III, Bloomington *Drosophila* Stock Center #43550, targeting Egl CDS 1590–1610 nt, 5′-CACGGTGATAGCGAATGTCAA-3′); *UASp-CFP-Msps.CDS* (from Dr. Timothy Megraw, Florida State University) (67); *Tub-PBac* (Bloomington *Drosophila* Stock Center #8285); *UASt-NbVHH05-EGFP* (attP40, II, Bloomington *Drosophila* stock center # 94008) (65); *UAS-Rhi-RNAi* (From Dr. Zhao Zhang, Duke University School of Medicine) (77); *ubi-Msps.CDS-GFP* (From Dr. Jordan Raff, University of Oxford) (66). The following transgenic fly stocks were generated in this study using PhiC31-mediated integration (BestGene Inc.): *UASp-sfGFP-msps 3′UTR and UASp-sfGFP-K10CT 3′UTR* (inserted at VK27, 89E11, III); *UASp-MoxMaple3-K10subregionA 3′UTR* and *UASp-Msps (RNAi-resistant)-MoxMaple3-K10subregionA 3′UTR* (inserted at VK05, 75A10, III); and *UASp-Msps (RNAi-resistant)-YFP-BLID-K10subregionA 3′UTR and UASp-Msps-TOG(1–4)-YFP-BLID-K10subregionA 3′UTR* (inserted at attP1, 55C4, II).

Plasmid Constructs.

-pUASp-attB-sfGFP-msps 3′UTR. *msps* 3′UTR were amplified from the genomic DNA and inserted into the pUASp-attB-ΔK10 (the original C terminus (CT) of K10 3′UTR and terminator region was replaced with *Drosophila* α-tubulin terminator and polyA signal, a kind gift from Paul Schedl, Princeton University) (78) via EcoRI(5′) and KpnI(3′) to create pUASp-attB-msps 3′UTR. sfGFP was amplified by PCR and inserted into the pUASp-attB-msps'3UTR via XbaI (5′) and EcoRI (3′) to create pUASp-attB-sfGFP-msps 3′UTR.

-pUASp-attB-sfGFP-K10CT 3′UTR. The K10CT 3′UTR (973 to 1489 nt, after HpaI site, without the subregion A or TLS that is required for oocyte transport and localization) (62) was amplified by PCR from the pUASp vector (79) and inserted into the pUASp-attB-sfGFP-msps 3′UTR via EcoRI(5′) and KpnI(3′) to replace the *msps* 3′UTR.

-pUASp-attB-MoxMaple3-K10subregionA 3′UTR. The MoxMaple3 were amplified from pUASp-Mito-MoxMaple3 construct (50) by PCR and inserted into pUASp-attB via SpeI(5′) and XbaI(3′). A small fragment of K10 3′UTR (Subregion A containing TLS, AGGCCTTAGATTACACCACTTGATTGTATTTTTAAATTAATTCTTAAAAACTACA

AATTAAGATCACTCTGTGAACGTGTGCTCGATGGTG) (62) was synthesized and inserted into the pUASp-attB-MoxMaple3 via PspXI single digestion to ensure the oocyte enrichment of the *MoxMaple3* mRNA.

-pUASp-attB-Msps (RNAi-resistant)-MoxMaple3- K10subregionA 3′UTR. Two DNA fragments carrying overlapping silent mutations of Msps protein isoform C (7225 to 7245 nt, TTAAGAGATTACGAGGAGATT, corresponding to 1636 to 1642 residues of LRDYEEI, RNAi-resistant to *UAS-msps-RNAi* TRiP line HMS01906 that targets 5′- CTGCGCGACTATGAAGAAATA-3′) were amplified from the pIZ-Msps-GFP construct (a kind gift from Steve Rogers, the University of North Carolina at Chapel Hill) (43) and inserted back into pIZ-Msps-GFP digested with SspI(5′) and XhoI(3′) using Infusion ligation (Takara Bio) to create pIZ-Msps (RNAi-resistant)-GFP. Msps (RNAi-resistant) was then subcloned into pUASp-attB-MoxMaple3 construct via NotI(5′) and SpeI(3′) to create pUASp-attB-Msps (RNAi-resistant)-MoxMaple3. A small fragment of K10 3′UTR (Subregion A containing TLS, GGCC TTAGATTACACCACTTGATTGTATTTTTAAATTAATTCTTAAAAACTACAAATTAAGATCACT CTGTGAACGTGTGCTCGATGGTG) (62) was synthesized and inserted into the pUASp-attB-Msps (RNAi-resistant)-MoxMaple3 via PspXI single digestion to ensure the oocyte enrichment of the *msps (RNAi-resistant)-MoxMaple3* mRNA.

-pUASp-attB-Msps (RNAi-resistant)-YFP-BLID-K10subregionA 3′UTR. YFP-BLID (sensitive to blue light; delete the last three amino acids from AsLOV2, with I532A mutation and RRRG degron) was amplified by PCR from pBMN-HA-YFP-LOV24 (Addgene, Plasmid #49570) (80) and inserted into the pUASp-attB vector via BamHI(5′) and XbaI(3′). Msps (RNAi-resistant) fragment was subcloned from pUASp-attB-Msps (RNAi-resistant)-MoxMaple3 into pUASp-attB-YFP-BLID via NotI (5′) and SpeI (3′). A small fragment of K10 3′UTR (Subregion A containing TLS, AGGCCTTAGATTACACCACTTGATTGTATTTTTAAATTAATTCTTAAAAACTACAAATTAA GATCACTCTGTGAACGTGTGCTCATGGTG) (62) was synthesized and inserted into the pUASp-attB-Msps (RNAi-resistant)-YFP-BLID via PspXI single digestion to ensure the oocyte enrichment of *msps (RNAi-resistant)-YFP-BLID* mRNA.

-pUASp-attB-Msps-TOG(1–4)-YFP-BLID-K10subregionA 3′UTR. Msps TOG(1–4) fragment (43) was amplified from pUASp-attB-Msps (RNAi-resistant)-YFP-BLID-K10subregionA 3′UTR and inserted into pUASp-attB-Msps (RNAi-resistant)-YFP-BLID-K10subregionA 3′UTR via PacI (5′) and SpeI (3′) to replace the full-length Msps (RNAi-resistant).

CRISPR Knock-In to Create *msps-3XVHH05-6XMS2*. Two small gRNAs (#1-GGGGTATTTCAATCAGAAGC; #2- ACGGGAAGCGCACAGTTTAT) targeting *msps* genomic region were synthesized and inserted into the pCFD5 vector (81) (Addgene, Plasmid #73914) via BbsI digestion. 6XMS2 were amplified from the pSL-MS2-6X (Addgene, plasmid #27118) (82) and inserted into the pScarlessHD-C-3xVHH05-DsRed (Addgene, Plasmid #171580) (65) via InFusion cloning (Takara Bio) to create the vector of pScarlessHD-C-3xVHH05-6XMS2-DsRed. ~1 kb 5′ homology arm and ~1 kb 3′ homology arm of *msps* genomic region were amplified from the genomic DNA (Sigma, Extract-N-Amp™ Tissue PCR Kit), mutated to be insensitive to gRNAs, and inserted into the pScarlessHD-C-3xVHH05-6XMS2-DsRed vector via InFusion cloning (Takara Bio). The DNA plasmid of pScarlessHD-5′ *msps* homology arm-C-3xVHH05-6XMS2-DsRed-3′ *msps* homology arm was coinjected with pCFD5-gRNA#1 and pCFD5-gRNA#2 by BestGene. Flies with red fluorescent eyes were selected and crossed with *Tub-PBac* flies to remove the DsRed region by PBac transposase. The final *msps-3XVHH05-6XMS2* line was verified using genomic PCR amplification and Sanger sequencing.

Live Imaging of *Drosophila* Egg Chambers. Young female adults were mated with several male flies and fed with active dry yeast for 16 to 18 h before dissection. The ovaries were dissected in Halocarbon oil 700 (Sigma-Aldrich, Cat# H8898) as previously described (10, 50, 61, 70, 83). Freshly dissected samples were imaged on a Nikon W1 spinning disk confocal microscope (Yokogawa CSU with pinhole size 50 μm) with a Hamamatsu ORCA-Fusion Digital CMOS Camera, and a 40× 1.25 N.A. silicone oil lens, controlled by Nikon Elements software.

Anti-Orb and anti-C(3)G Immunostaining in *Drosophila* Egg Chambers. A standard fixation and immunostaining protocol was described previously (10, 50, 61, 70, 73, 83). Young female adults were mated with several male flies and fed with active dry yeast for 16 to 18 h before dissection. Ovaries were dissected in 1X PBS and fixed with 4% EM-grade formaldehyde (Electron Microscopy Sciences 16% Paraformaldehyde Aqueous Solution, Fisher Scientific, Cat# 50-980-487) in 1× PBS +0.1% Triton X-100 for 20 min on a rotator at room temperature; washed with 1× PBTB (1X PBS +0.1% Triton X-100+0.2% BSA) five times for 10 min each time, and blocked in 5% (vol/vol) normal goat serum-containing 1× PBTB for 1h at RT; stained with the primary mouse monoclonal anti-Orb antibody (Orb 4H8, Developmental Studies Hybridoma Bank, supernatant, 1:5), or mouse anti-C(3)G [1A8-1G2, 1:500 (53) at 4 °C overnight; washed with 1× PBTB five times for 10 min each time; stained with the FITC-conjugated or TRITC-conjugated anti-mouse secondary antibody (Jackson ImmunoResearch Laboratories, Inc; Cat# 115-095-062 and Cat# 115-025-003) at 10 μg/mL at room temperature (24 to 25 °C) for 4 h; stained with rhodamine-conjugated or Alexa Fluor633-conjugated phalloidin (0.2 μg/mL), and DAPI (1 μg/mL) for >1 h at room temperature, and washed with 1× PBTB five times for 10 min each time before mounting. Samples were imaged on a Nikon A1plus scanning confocal microscope with a GaAsP detector and a 20× 0.75 N.A. lens using Galvano scanning (for anti-Orb staining), or on a Nikon W1 spinning disk confocal microscope (Yokogawa CSU with pinhole size 50 μm) with a Hamamatsu ORCA-Fusion Digital CMOS Camera, and a 40× 1.25 N.A. silicone oil lens (for anti-C(3)G staining), controlled by Nikon Elements software. Z-stack images were acquired every 1 μm/step (for anti-Orb staining) or every 0.5 μm/step (for anti-C(3)G staining).

Microtubule Staining in *Drosophila* Egg Chambers. Ovaries were dissected in 1× Brinkley Renaturing Buffer 80 [BRB80, 80 mM piperazine-N,N′-bis(2-ethanesulfonic acid) (PIPES), 1 mM MgCl2, 1 mM EGTA, pH 6.8] and fixed in 8% EM-grade formaldehyde (Electron Microscopy Sciences 16% Paraformaldehyde Aqueous Solution, Fisher Scientific, Cat# 50-980-487) +1× BRB80 +0.1% Triton X-100 for 20 min on a rotator at room temperature; briefly washed with 1X PBTB (1× PBS + 0.1% Triton X-100 +0.2% BSA) five times for 10 min each time, and blocked in 5% (vol/vol) normal goat serum-containing 1× PBTB for 1 h at room temperature; stained with CoraLitePlus 488-conjugated or CoraLite594-conjugated β-tubulin monoclonal antibody (ProteinTech, Cat# CL488-66240, Clone No. 1D4A4; Cat# CL594-66240, Clone No. 1D4A4) 1:100 at 4 °C overnight; samples were stained rhodamine-conjugated or Alexa Fluor633-conjugated phalloidin (0.2 μg/mL), and DAPI (1 μg/mL) for 1 h before mounting. Samples were imaged using a Nikon W1 spinning disk confocal microscope (Yokogawa CSU with pinhole size 50 μm) with a Hamamatsu ORCA-Fusion Digital CMOS Camera and a 100× 1.35 N.A. silicone oil lens, controlled by Nikon Elements software. Images were acquired every 0.5 μm/step in z stacks.

Ovaries from flies expressing maternal αtub67C-EMTB-3XGFP-sqh 3'UTR were dissected in 1× BRB80 buffer and fixed in 8% EM-grade formaldehyde +1× BRB80 +0.1% Triton X-100 for 20 min on a rotator, briefly washed with 1× PBTB five times for 10 min each time, and stained rhodamine-conjugated phalloidin (0.2 μg/mL) and DAPI (1 μg/mL) for 1 h before mounting. Samples were imaged using a Nikon W1 spinning disk confocal microscope (Yokogawa CSU with pinhole size 50 μm) with a Hamamatsu ORCA-Fusion Digital CMOS Camera and a 100× 1.35 N.A. silicone oil lens, controlled by Nikon Elements software. Images were acquired every 0.5 μm/step in z stacks.

Single-Molecule Inexpensive Fluorescence in situ Hybridization (smiFISH). The smiFISH protocol was based on (84–86) with some small modifications. Twenty-base-long DNA probes complementary to the mRNA of *msps* 3′UTR, sfGFP, CFP, MoxMaple3, or YFP with 3′ FLAP-X complementary probe (5′-CCTCCTAAG TTTCGAGCTGGACTCAGTG-3′) were designed using LGC Biosearch Technologies' Stellaris RNA FISH Probe Designer (masking level five, minimal spacing two bases). Twenty five probes specific to *msps* 3′UTR mRNA and 10 probes specific to sfGFP, CFP, MoxMaple3, and YFP mRNAs were ordered from ThermoFisher (25 nmol synthesis scale, standard desalting) (the probe sequences are listed in *SI Appendix*, Table S1) and diluted to 100 μM in nuclease-free H2O. Probes were mixed at equal molar ratios (to a mixed probe concentration of 100 μM) and stored at −20 °C. Fluorescently labeled Flap-X probe with 5′ and 3′ Cy5 modifications (/5Cy5/CACTGAGTCCAGCTCGAAACTTAGGAGG-/3Cy5Sp/) was ordered from IDT (100 nmol synthesis scale, HPLC purified), diluted in nuclease-free H2O to a concentration of 100 μM, and stored at −20 °C in aliquots. mRNA-FLAP-X complementary probes and fluorescent Flap-X probes were annealed by mixing 2 μL of mixed mRNA-FLAP-X complementary probe (100 μM mixed concentration), 2.5 μL of Cy5-FlapX probe (100 μM), 5 μL of New England Biolabs Buffer 3 (1× composition: 100 mM NaCl, 50 mM Tris-HCl, 10 mM MgCl2, 1mM DTT, pH 7.9), and 40.5 μL nuclease-free H2O, incubated at 85 °C for 3 min, 65 °C for 3 min, and 25 °C for 5 min in a PCR machine, and stored at −20 °C.

Ovaries were 1) dissected in 1× PBS and fixed in 4% EM-grade formaldehyde (Electron Microscopy Sciences 16% Paraformaldehyde Aqueous Solution, Fisher Scientific, Cat#50-980-487) in 1× PBST (1× PBS +0.1% Triton X-100 in nuclease-free H_2O) for 20 min on a rotator at room temperature; 2) washed three times in 1× PBST for 5 min each at room temperature; 3) exchanged into a 1:1 volume mixture of 1× PBST and smiFISH Wash Buffer [10% 20× SSC (20× SSC: 0.3M sodium citrate, 3M NaCl, in nuclease-free H_2O, pH7.0), 10% deionized formamide, in nuclease-free water], and incubated at room temperature for 10 min; 4) washed two times in smiFISH Wash Buffer for 10 min each at room temperature; 5) incubated at 37 °C in smiFISH Wash Buffer for 30 min; 6) incubated with 2 μL annealed probe diluted in 500 μL 37 °C-prewarmed smiFISH Hybridization Buffer (10% dextran sulfate, 10% 20× SSC, 10% deionized formamide, in nuclease-free water) overnight (>16 h) at 37 °C in dark; 7) diluted with 500 μL 37 °C-prewarmed smiFISH Wash Buffer; 8) washed three times in smiFISH Wash Buffer for 10 min each at 37 °C; 9) incubated at room temperature in a 1:1 volume mixture of 1× PBST and smiFISH Wash Buffer for 10 min; 10) incubated in 1× PBST with rhodamine-conjugated phalloidin (0.2 μg/mL) and DAPI (1 μg/mL) for 1 h; 11) washed two times in 1× PBST at room temperature for 10 min each before mounting.

Measurement of Nurse Cell and Oocyte Size. Z stacks of triple color images of the ovarioles stained with DAPI, anti-Orb antibody, and rhodamine-conjugated phalloidin were acquired on a Nikon A1plus scanning confocal microscope with a GaAsP detector and a 20× 0.75 N.A. lens using Galvano scanning, at every 1 μm/step. Egg chamber stages' characterization was previously described (50, 87). Nurse cell area and oocyte area were specified (at the largest cross-section) and measured by manual polygon selection (area size) in FIJI.

Quantification of smiFISH Staining. Z stack images of the ovarioles stained with DAPI, rhodamine-conjugated phalloidin, and Cy5-labeled FLAP-X smiFISH probe (some samples were also labeled with YFP) were acquired on a Nikon W1 spinning disk confocal microscope (Yokogawa CSU with pinhole size 50 μm) with a Hamamatsu ORCA-Fusion Digital CMOS Camera, and a 40× 1.25 N.A. silicone oil lens, at every 0.5 μm/step. Egg chamber stages' characterization was previously described (50, 87). A sum Z-projection of a total 2.5 μm z-stack image (six z-slices in total) of each egg chamber was created by FIJI (Image>Stacks>Z projection>Sum slices), and cell area and fluorescence intensity were measured by manual polygon selection in FIJI.

Quantification of Microtubule Staining in *Drosophila* Egg Chambers. Z stacks of triple color images of the ovarioles stained with DAPI, rhodamine-conjugated phalloidin, and FITC-conjugated β-tubulin or EMTB-3XGFP labeling were acquired on a Nikon W1 spinning disk confocal microscope (Yokogawa CSU with pinhole size 50 μm) with a Hamamatsu ORCA-Fusion Digital CMOS Camera, with a 100× 1.35 N.A. silicone oil lens, at every 0.5 μm/step. Egg chamber stages' characterization was previously described (50, 87). A sum Z-projection of a total 2.5 μm z-stack image (six z-slices in total) of a stage 6 to 7 egg chamber was created by FIJI (Image>Stacks>Z projection>Sum slices), and cell area and fluorescence intensity were measured by manual polygon selection in FIJI.

EB1 Comet Tracking in *Drosophila* Egg Chambers. *ubi-EB1-GFP* time-lapse movies of stage 6 to 8 egg chambers in either control or *msps-RNAi* were acquired on a Nikon W1 spinning disk confocal microscope (Yokogawa CSU with pinhole size 50 μm) with a Hamamatsu ORCA-Fusion Digital CMOS Camera, and a 40× 1.25 N.A. silicone oil lens, at a frame rate of every 2 s for a total of 2 min, controlled by Nikon Elements software. Images were processed in FIJI and analyzed in DiaTrack 3.04 Pro (88), with a maximal particle jump distance of 0.57 μm/s, a minimal speed limit of 0.01 μm/s, and a minimal lifetime of 6 s. The sum of the length of EB1-GFP tracks was considered to be the total length of newly polymerized microtubules. For each sample, both the number of EB1 comets and the length of newly polymerized microtubules are normalized by the cell area size to get the EB1 density (#/μm^2) and the new microtubule length per min (μm/μm^2).

Quantification of NbVHH05 Staining. Samples of 1) *yw/w; UASt-NbVHH05-EGFP/+; Msps-3XVHH05/mat αtub-Gal4$^{[V37]}$, UAS-Rhi-RNAi* [*Rhi-RNAi* increases the UASt-NbVHH05 expression in the germ line (77) (control); 2) *yw/w; UASt-NbVHH05-EGFP/+; mat αtub-Gal4$^{[V37]}$, UAS-Rhi-RNAi/+* (Nb only); 3) *yw/w; UASt-NbVHH05-EGFP/UAS-Dhc-RNAi; Msps-3XVHH05/mat αtub-Gal4$^{[V37]}$, UAS-Rhi-RNAi* (*Dhc-RNAi*) were dissected in 1X PBS and fixed with 4% EM-grade formaldehyde in 1× PBS +0.1% Triton X-100 for 20 min on a rotator at room temperature; washed with 1X PBTB (1× PBS + 0.1% Triton X-100 +0.2% BSA) five times for 10 min each time, and stained with rhodamine-conjugated phalloidin (0.2 μg/mL) and DAPI (1 μg/mL) for >1 h before mounting. Samples were imaged on a Nikon W1 spinning disk confocal microscope (Yokogawa CSU with pinhole size 50 μm) with a Hamamatsu ORCA-Fusion Digital CMOS Camera, with a 40× 1.25 N.A. silicone oil lens, at every 0.5 μm/step. Egg chamber stages' characterization was previously described (50, 87). A sum Z-projection of a total 5 μm z-stack image (11 z-slices in total) of each egg chamber was created by FIJI (Image>Stacks>Z projection>Sum slices), and cell area and fluorescence intensity were measured by manual polygon selection in FIJI.

Photoconversion of MoxMaple3 and Msps-MoxMaple3. Young mated female adults of 1) *yw; mat αtub-Gal4$^{[V37]}$/UASp-MoxMaple3-K10.TLS,* 2) *yw; mat αtub-Gal4$^{[V37]}$/UASp-Msps-MoxMaple3-K10.TLS*, and 3) *yw; UASp-Klp10A-GFP-SspB/+; mat αtub-Gal4$^{[V37]}$/UASp-Msps-MoxMaple3-K10.TLS* were dissected in Halocarbon oil 700, as described above. Freshly dissected samples were imaged on a Nikon W1 spinning disk confocal microscope (Yokogawa CSU with pinhole size 50 μm) with a Hamamatsu ORCA-Fusion Digital CMOS Camera and a 40× 1.25 N.A. silicone oil lens. MoxMaple3 was photoconverted from green to red within a circle of ~12 μm diameter inside the oocytes by 405 nm light controlled by Mightex Polygon DMD Illuminator. The photoconverted signal was acquired at 0.5 μm/step in Z-stack images after photoconversion. Sum slices of the Z projection were used to calculate the nurse cell-to-oocyte ratio of the average intensity of the photoconverted signal.

Anti-Msps Antibody Staining. The rabbit crude serum containing the polyclonal antibody against *Drosophila* Msps TOG2 domain (a kind gift from Steve Rogers, UNC at Chapel Hill) (43) was preadsorbed twice with wild-type ovaries (fixed with 4% EM-grade formaldehyde, but not blocked) at 1:10 dilution at 4 °C for overnight to reduce the nonspecific background. The preabsorbed anti-Msps antibody was then diluted 1:5 in overnight staining (final dilution at 1:50) at 4 °C. FITC-conjugated anti-rabbit secondary antibody (Jackson ImmunoResearch Laboratories, Inc; Cat#111-095-003) was used at 10 μg/mL at room temperature for 4 h before washing and mounting. Samples were imaged on a Nikon W1 spinning disk confocal microscope (Yokogawa CSU with pinhole size 50 μm) with a Hamamatsu ORCA-Fusion Digital CMOS Camera and a 40× 1.25 N.A. silicone oil lens at every 0.5 μm/step.

Statistical Analysis. The figures plots show either percentage of phenotypes or mean values, as indicated in figure legends. Error bars represent 95% CI and N stands for sample numbers examined in each assay. Statistical analysis was performed in GraphPad Prism 8.0.2. *P* values are calculated using unpaired *t* tests with Welch's correction, and the levels of statistical significance are assigned as follows: $P \geq 0.05$, not significant (n.s.); $0.01 \leq P < 0.05$, significant (*); $0.001 \leq P < 0.01$, very significant (**); P 0.0001 $\leq P < 0.001$, extremely significant (***); $P < 0.0001$, extremely significant (****).

Data, Materials, and Software Availability. All study data are included in the article and/or supporting information.

ACKNOWLEDGMENTS. We thank many colleagues who generously contributed reagents for this work: Dr. Steve Rogers (UNC at Chapel Hill), Dr. Antoine Guichet (CNRS, Institut Jacques Monod), Dr. David Glover (Caltech), Dr. Yu-Chiun Wang (RIKEN Center for Biosystems Dynamics Research, Japan), Dr. Graydon Gonsalvez (Augusta University), Dr. Timothy Megraw (Florida State University), Dr. Jordan Raff (University of Oxford), Dr. Zhao Zhang (Duke University School of Medicine), Dr. Paul Schedl (Princeton University), Dr. Scott Hawley (Stowers Institute), and Bloomington *Drosophila* Stock Center (supported by NIH grant P40OD018537) for fly stocks. The Orb 4H8 monoclonal antibody developed by Dr. Paul D. Schedl's group at Princeton University was obtained from the Developmental Studies Hybridoma Bank, created by the NICHD of the NIH and maintained at the University of Iowa. We thank Northwestern Center for Advanced Microscopy & Nikon Imaging Center for imaging assistance and Northwestern Sanger Sequencing Facility for sequencing services. We thank all the Gelfand laboratory members for their support, discussion, and suggestions. Research reported in this study was supported by the National Institute of General Medical Sciences grant R35GM131752 to V.I.G.

1. K. Lu, L. Jensen, L. Lei, Y. M. Yamashita, Stay connected: A germ cell strategy. *Trends Genet.* **33**, 971–978 (2017).
2. W. Lu, V. I. Gelfand, Go with the flow – bulk transport by molecular motors. *J. Cell Sci.* **136**, jcs260300 (2023).
3. M. P. Greenbaum, T. Iwamori, G. M. Buchold, M. M. Matzuk, Germ cell intercellular bridges. *Cold Spring Harb. Perspect. Biol.* **3**, a005850 (2011).
4. K. Haglund, I. P. Nezis, H. Stenmark, Structure and functions of stable intercellular bridges formed by incomplete cytokinesis during development. *Commun. Integr. Biol.* **4**, 1–9 (2011).
5. M. Buszczak, L. Cooley, Eggs to die for: Cell death during Drosophila oogenesis. *Cell Death Differ.* **7**, 1071–1074 (2000).
6. L. Lei, A. C. Spradling, Mouse oocytes differentiate through organelle enrichment from sister cyst germ cells. *Science* **352**, 95–99 (2016).
7. T. D. Hinnant, J. A. Merkle, E. T. Ables, Coordinating proliferation, polarity, and cell fate in the Drosophila female germline. *Front. Cell Dev. Biol.* **8**, 19 (2020).
8. R. Bastock, D. St Johnston, Drosophila oogenesis. *Curr. Biol.* **18**, R1082–R1087 (2008).
9. E. A. Koch, P. A. Smith, R. C. King, The division and differentiation of Drosophila cystocytes. *J. Morphol.* **121**, 55–70 (1967).
10. W. Lu, M. Lakonishok, A. S. Serpinskaya, V. I. Gelfand, A novel mechanism of bulk cytoplasmic transport by cortical dynein in Drosophila ovary. *ELife* **11**, e75538 (2022).
11. W. E. Theurkauf, B. M. Alberts, Y. N. Jan, T. A. Jongens, A central role for microtubules in the differentiation of Drosophila oocytes. *Development* **118**, 1169–1180 (1993).
12. W. E. Theurkauf, S. Smiley, M. L. Wong, B. M. Alberts, Reorganization of the cytoskeleton during Drosophila oogenesis: Implications for axis specification and intercellular transport. *Development* **115**, 923–936 (1992).
13. E. A. Koch, R. H. Spitzer, Multiple effects of colchicine on oogenesis in Drosophila: Induced sterility and switch of potential oocyte to nurse-cell developmental pathway. *Cell Tissue Res.* **228**, 21–32 (1983).
14. J. Bolivar *et al.*, Centrosome migration into the Drosophila oocyte is independent of BicD and egl, and of the organisation of the microtubule cytoskeleton. *Development* **128**, 1889–1897 (2001).
15. D. Nashchekin, L. Busby, M. Jakobs, I. Squires, D. St Johnston, Symmetry breaking in the female germline cyst. *Science* **374**, 874–879 (2021).
16. W. M. Saxton, Microtubules, motors, and mRNA localization mechanisms: Watching fluorescent messages move. *Cell* **107**, 707–710 (2001).
17. M. M. L. Tillery, C. Blake-Hedges, Y. Zheng, R. A. Buchwalter, T. L. Megraw, Centrosomal and non-centrosomal microtubule-organizing centers (MTOCs) in Drosophila melanogaster. *Cells* **7**, 121 (2018).
18. M. Li, M. McGrail, M. Serr, T. S. Hays, Drosophila cytoplasmic dynein, a microtubule motor that is asymmetrically localized in the oocyte. *J. Cell Biol.* **126**, 1475–1494 (1994).
19. M. McGrail, T. S. Hays, The microtubule motor cytoplasmic dynein is required for spindle orientation during germline cell divisions and oocyte differentiation in Drosophila. *Development* **124**, 2409–2419 (1997).
20. M. Mcgrail *et al.*, Regulation of cytoplasmic dynein function in-vivo by the drosophila glued complex. *J. Cell Biol.* **131**, 411–425 (1995).
21. S. Mische *et al.*, Dynein light intermediate chain: An essential subunit that contributes to spindle checkpoint inactivation. *Mol. Biol. Cell* **19**, 4918–4929 (2008).
22. C. Navarro, H. Puthalakath, J. M. Adams, A. Strasser, R. Lehmann, Egalitarian binds dynein light chain to establish oocyte polarity and maintain oocyte fate. *Nat. Cell Biol.* **6**, 427–435 (2004).
23. J. Januschke *et al.*, Polar transport in the Drosophila oocyte requires dynein and Kinesin I cooperation. *Curr. Biol.* **12**, 1971–1981 (2002).
24. Z. Liu, T. Xie, R. Steward, Lis1, the Drosophila homolog of a human lissencephaly disease gene, is required for germline cell division and oocyte differentiation. *Development* **126**, 4477–4488 (1999).
25. B. Suter, L. M. Romberg, R. Steward, Bicaudal-D, a Drosophila gene involved in developmental asymmetry: Localized transcript accumulation in ovaries and sequence similarity to myosin heavy chain tail domains. *Genes Dev.* **3**, 1957–1968 (1989).
26. T. Schupbach, E. Wieschaus, Female sterile mutations on the second chromosome of Drosophila melanogaster. II. Mutations blocking oogenesis or altering egg morphology. *Genetics* **129**, 1119–1136 (1991).
27. J. M. Mach, R. Lehmann, An Egalitarian-BicaudalD complex is essential for oocyte specification and axis determination in Drosophila. *Genes Dev.* **11**, 423–435 (1997).
28. J. Oh, R. Steward, Bicaudal-D is essential for egg chamber formation and cytoskeletal organization in drosophila oogenesis. *Dev. Biol.* **232**, 91–104 (2001).
29. R. J. McKenney, W. Huynh, M. E. Tanenbaum, G. Bhabha, R. D. Vale, Activation of cytoplasmic dynein motility by dynactin–cargo adapter complexes. *Science* **345**, 337–341 (2014).
30. S. L. Reck-Peterson, W. B. Redwine, R. D. Vale, A. P. Carter, The cytoplasmic dynein transport machinery and its many cargoes. *Nat. Rev. Mol. Cell Biol.* **19**, 382–398 (2018).
31. P. Sanghavi, G. Liu, R. Veeranan-Karmegam, C. Navarro, G. B. Gonsalvez, Multiple roles for egalitarian in polarization of the drosophila egg chamber. *Genetics* **203**, 415–432 (2016).
32. C. H. Goldman, H. Neiswender, R. Veeranan-Karmegam, G. B. Gonsalvez, The egalitarian binding partners dynein light chain and Bicaudal-D act sequentially to link mRNA to the dynein motor. *Development* **146**, dev176529 (2019).
33. C. H. Goldman *et al.*, Optimal RNA binding by egalitarian, a dynein cargo adaptor, is critical for maintaining oocyte fate in Drosophila. *RNA Biol.* **18**, 2376–2389 (2021).
34. M. Dienstbier, F. Boehl, X. Li, S. L. Bullock, Egalitarian is a selective RNA-binding protein linking mRNA localization signals to the dynein motor. *Genes Dev.* **23**, 1546–1558 (2009).
35. H. Neiswender, C. H. Goldman, R. Veeranan-Karmegam, G. B. Gonsalvez, Dynein light chain–dependent dimerization of Egalitarian is essential for maintaining oocyte fate in Drosophila. *Dev. Biol.* **478**, 76–88 (2021).
36. P. Vazquez-Pianzola *et al.*, The mRNA transportome of the BicD/Egl transport machinery. *RNA Biol.* **14**, 73–89 (2017).
37. D. L. Gard, M. W. Kirschner, A microtubule-associated protein from Xenopus eggs that specifically promotes assembly at the plus-end. *J. Cell Biol.* **105**, 2203–2215 (1987).
38. G. J. Brouhard *et al.*, XMAP215 is a processive microtubule polymerase. *Cell* **132**, 79–88 (2008).
39. J. Al-Bassam, N. A. Larsen, A. A. Hyman, S. C. Harrison, Crystal structure of a TOG domain: Conserved features of XMAP215/Dis1-family TOG domains and implications for tubulin binding. *Structure* **15**, 355–362 (2007).
40. K. C. Slep, R. D. Vale, Structural basis of microtubule plus end tracking by XMAP215, CLIP-170, and EB1. *Mol. Cell* **27**, 976–991 (2007).
41. K. C. Slep, The role of TOG domains in microtubule plus end dynamics. *Biochem. Soc. Trans.* **37**, 1002–1006 (2009).
42. A. E. Byrnes, K. C. Slep, TOG-tubulin binding specificity promotes microtubule dynamics and mitotic spindle formation. *J. Cell Biol.* **216**, 1641–1657 (2017).
43. J. D. Currie *et al.*, The microtubule lattice and plus-end association of Drosophila mini spindles is spatially regulated to fine-tune microtubule dynamics. *Mol. Biol. Cell* **22**, 4343–4361 (2011).
44. B. van der Vaart *et al.*, SLAIN2 links microtubule plus end-tracking proteins and controls microtubule growth in interphase. *J. Cell Biol.* **193**, 1083–1099 (2011).
45. W. Li *et al.*, EB1 promotes microtubule dynamics by recruiting sentin in Drosophila cells. *J. Cell Biol.* **193**, 973–983 (2011).
46. C. F. Cullen, P. Deak, D. M. Glover, H. Ohkura, mini spindles: A gene encoding a conserved microtubule-associated protein required for the integrity of the mitotic spindle in Drosophila. *J. Cell Biol.* **146**, 1005–1018 (1999).
47. C. F. Cullen, H. Ohkura, Msps protein is localized to acentrosomal poles to ensure bipolarity of Drosophila meiotic spindles. *Nat. Cell Biol.* **3**, 637–642 (2001).
48. G. Goshima, R. Wollman, N. Stuurman, J. M. Scholey, R. D. Vale, Length control of the metaphase spindle. *Curr. Biol.* **15**, 1979–1988 (2005).
49. W. Moon, T. Hazelrigg, The Drosophila microtubule-associated protein mini spindles is required for cytoplasmic microtubules in oogenesis. *Curr. Biol.* **14**, 1957–1961 (2004).
50. W. Lu, M. Lakonishok, V. I. Gelfand, Gatekeeper function for short stop at the ring canals of the Drosophila ovary. *Curr. Biol.* **31**, 3207–3220.e4 (2021), 10.1016/j.cub.2021.05.010.
51. M. Van Doren, A. L. Williamson, R. Lehmann, Regulation of zygotic gene expression in Drosophila primordial germ cells. *Curr. Biol.* **8**, 243–246 (1998).
52. V. Lantz, J. S. Chang, J. I. Horabin, D. Bopp, P. Schedl, The Drosophila Orb Rna-binding protein is required for the formation of the egg chamber and establishment of polarity. *Genes Dev.* **8**, 598–613 (1994).
53. L. K. Anderson *et al.*, Juxtaposition of C(2)M and the transverse filament protein C(3)G within the central region of Drosophila synaptonemal complex. *Proc. Natl. Acad. Sci. U.S.A.* **102**, 4482–4487 (2005).
54. K. A. Collins *et al.*, Corolla is a novel protein that contributes to the architecture of the synaptonemal complex of Drosophila. *Genetics* **198**, 219–228 (2014).
55. Y. Komarova *et al.*, Mammalian end binding proteins control persistent microtubule growth. *J. Cell Biol.* **184**, 691–706 (2009).
56. W. Lu, M. Lakonishok, V. I. Gelfand, Kinesin-1-powered microtubule sliding initiates axonal regeneration in Drosophila cultured neurons. *Mol. Biol. Cell* **26**, 1296–1307 (2015).
57. U. Del Castillo, M. Winding, W. Lu, V. I. Gelfand, Interplay between kinesin-1 and cortical dynein during axonal outgrowth and microtubule organization in Drosophila neurons. *eLife* **4**, e10140 (2015).
58. Y. Shimada, S. Yonemura, H. Ohkura, D. Strutt, T. Uemura, Polarized transport of frizzled along the planar microtubule arrays in Drosophila wing epithelium. *Dev. Cell* **10**, 209–222 (2006).
59. G. Goshima, R. D. Vale, Cell cycle-dependent dynamics and regulation of mitotic kinesins in Drosophila S2 cells. *Mol. Biol. Cell* **16**, 3896–3907 (2005).
60. V. Mennella *et al.*, Functionally distinct kinesin-13 family members cooperate to regulate microtubule dynamics during interphase. *Nat. Cell Biol.* **7**, 235–245 (2005).
61. W. Lu *et al.*, Competition between kinesin-1 and myosin-V defines Drosophila posterior determination. *eLife* **9**, e54216 (2020).
62. T. L. Serano, R. S. Cohen, A small predicted stem–loop structure mediates oocyte localization of Drosophila K10 mRNA. *Development* **121**, 3809–3818 (1995).
63. V. Van De Bor, E. Hartswood, C. Jones, D. Finnegan, I. Davis, Gurken and the I factor retrotransposon RNAs share common localization signals and machinery. *Dev. Cell* **9**, 51–62 (2005).
64. S. L. Bullock, D. Zicha, D. Ish-Horowicz, The Drosophila hairy RNA localization signal modulates the kinetics of cytoplasmic mRNA transport. *EMBO J.* **22**, 2484–2494 (2003).
65. J. Xu *et al.*, Protein visualization and manipulation in Drosophila through the use of epitope tags recognized by nanobodies. *eLife* **11**, e74326 (2022).
66. M. J. Lee, F. Gergely, K. Jeffers, S. Y. Peak-Chew, J. W. Raff, Msps/XMAP215 interacts with the centrosomal protein D-TACC to regulate microtubule behaviour. *Nat. Cell Biol.* **3**, 643–649 (2001).
67. Y. Zheng *et al.*, A perinuclear microtubule-organizing centre controls nuclear positioning and basement membrane secretion. *Nat. Cell Biol.* **22**, 297–309 (2020).
68. M. A. McClintock *et al.*, RNA-directed activation of cytoplasmic dynein-1 in reconstituted transport RNPs. *eLife* **7**, e36312 (2018).
69. J. C. Fox, A. E. Howard, J. D. Currie, S. L. Rogers, K. C. Slep, The XMAP215 family drives microtubule polymerization using a structurally diverse TOG array. *Mol. Biol. Cell* **25**, 2375–2392 (2014).
70. W. Lu, M. Winding, M. Lakonishok, J. Wildonger, V. I. Gelfand, Microtubule–microtubule sliding by kinesin-1 is essential for normal cytoplasmic streaming in Drosophila oocytes. *Proc. Natl. Acad. Sci. U.S.A.* **113**, E4995–5004 (2016).
71. N. C. Grieder, M. de Cuevas, A. C. Spradling, The fusome organizes the microtubule network during oocyte differentiation in Drosophila. *Development* **127**, 4253–4264 (2000).
72. R. Diegmiller, J. Imran Alsous, D. Li, Y. M. Yamashita, S. Y. Shvartsman, Fusome topology and inheritance during insect gametogenesis. *PLoS Comput. Biol.* **19**, e1010875 (2023).
73. W. Lu *et al.*, Niche-associated activation of rac promotes the asymmetric division of Drosophila female germline stem cells. *PLoS Biol.* **10**, e1001357 (2012).
74. K. Legent, N. Tissot, A. Guichet, Visualizing microtubule networks during drosophila oogenesis using fixed and live imaging. *Methods Mol. Biol.* **1328**, 99–112 (2015).
75. G. Minestrini, E. Mathe, D. M. Glover, Domains of the Pavarotti kinesin-like protein that direct its subcellular distribution: Effects of mislocalisation on the tubulin and actin cytoskeleton during Drosophila oogenesis. *J. Cell Sci.* **115**, 725–736 (2002).
76. G. Liu *et al.*, Efficient endocytic uptake and maturation in drosophila oocytes requires dynamitin/p50. *Genetics* **201**, 631–649 (2015).
77. S. Z. DeLuca, A. C. Spradling, Efficient expression of genes in the drosophila germline using a UAS promoter free of interference by Hsp70 piRNAs. *Genetics* **209**, 381–387 (2018).
78. J. Barr, R. Gilmutdinov, L. Wang, Y. Shidlovskii, P. Schedl, The Drosophila CPEB protein Orb Specifies oocyte fate by a 3′UTR-dependent autoregulatory loop. *Genetics* **213**, 1431–1446 (2019).
79. P. Rorth, Gal4 in the Drosophila female germline. *Mech. Dev.* **78**, 113–118 (1998).
80. K. M. Bonger, R. Rakhit, A. Y. Payumo, J. K. Chen, T. J. Wandless, General method for regulating protein stability with light. *Acs Chem. Biol.* **9**, 111–115 (2014).

81. F. Port, S. L. Bullock, Augmenting CRISPR applications in Drosophila with tRNA-flanked sgRNAs. *Nat. Methods* **13**, 852–854 (2016).
82. E. Bertrand *et al.*, Localization of ASH1 mRNA particles in living yeast. *Mol. Cell* **2**, 437–445 (1998).
83. W. Lu *et al.*, Ooplasmic flow cooperates with transport and anchorage in Drosophila oocyte posterior determination. *J. Cell Biol.* **217**, 3497–3511 (2018).
84. N. Tsanov *et al.*, smiFISH and FISH-quant - a flexible single RNA detection approach with super-resolution capability. *Nucleic Acids Res.* **44**, e165 (2016).
85. L. Calvo, M. Ronshaugen, T. Pettini, smiFISH and embryo segmentation for single-cell multi-gene RNA quantification in arthropods. *Commun. Biol.* **4**, 352 (2021).
86. A. L. Zajac, S. Horne-Badovinac, Kinesin-directed secretion of basement membrane proteins to a subdomain of the basolateral surface in Drosophila epithelial cells. *Curr. Biol.* **32**, 735–748.e10 (2022).
87. D. Jia, Q. Xu, Q. Xie, W. Mio, W. M. Deng, Automatic stage identification of Drosophila egg chamber based on DAPI images. *Sci. Rep.* **6**, 18850 (2016).
88. P. Vallotton, S. Olivier, Tri-track: Free software for large-scale particle tracking. *Microsc. Microanal.* **19**, 451–460 (2013).
89. W. Lu, M. Lakonishok, V. I. Gelfand, Drosophila oocyte specification is maintained by the dynamic duo of microtubule polymerase Mini spindles/XMAP215 and dynein. bioRxiv [Preprint] (2023). 10.1101/2023.03.09.531953 (Accessed 10 March 2023).